Coupled simulations of the Indian monsoon intraseasonal oscillation with a fine-resolution mixed-layer ocean model

Nicholas P. Klingaman, Hilary Weller, Steven J. Woolnough, Peter M. Inness, Julia M. Slingo

Walker Institute for Climate System Research and Department of Meteorology
University of Reading, P.O. Box 243, Reading, Berkshire RG6 6BB, United Kingdom
E-mail: n.p.klingaman@rdg.ac.uk

ABSTRACT

The intraseasonal variability (ISV) of the Indian summer monsoon is dominated by a 30–50 day oscillation between "active" and "break" events of enhanced and reduced rainfall over the subcontinent, respectively. These organized convective events form in the equatorial Indian Ocean and propagate north to India. Atmosphere–ocean coupled processes are thought to play a key role the intensity and propagation of these events.

A high-resolution, coupled atmosphere–mixed-layer-ocean model is assembled: HadKPP. HadKPP comprises the Hadley Centre Atmospheric Model (HadAM3) and the K Profile Parameterization (KPP) mixed-layer ocean model. Following studies that upper-ocean vertical resolution and sub-diurnal coupling frequencies improve the simulation of ISV in SSTs, KPP is run at 1 m vertical resolution near the surface; the atmosphere and ocean are coupled every three hours.

HadKPP accurately simulates the 30–50 day ISV in rainfall and SSTs over India and the Bay of Bengal, respectively, but suffers from low ISV on the equator. This is due to the HadAM3 convection scheme producing limited ISV in surface fluxes. HadKPP demonstrates little of the observed northward propagation of intraseasonal events, producing instead a standing oscillation. The lack of equatorial ISV in convection in HadAM3 constrains the ability of KPP to produce equatorial SST anomalies, which further weakens the ISV of convection. It is concluded that while atmosphere–ocean interactions are undoubtedly essential to an accurate simulation of ISV, they are not a panacea for model deficiencies.

In regions where the atmospheric forcing is adequate, such as the Bay of Bengal, KPP produces SST anomalies that are comparable to the Tropical Rainfall Measuring Mission Microwave Imager (TMI) SST analyses in both their magnitude and their timing with respect to rainfall anomalies over India. HadKPP also displays a much-improved phase relationship between rainfall and SSTs over a HadAM3 ensemble forced by observed SSTs, when both are compared to observations. Coupling to mixed-layer models such as KPP has the potential to improve operational predictions of ISV, particularly when the persistence time of SST anomalies is shorter than the forecast lead time.

1 Introduction

1.1 The northward-propagating intraseasonal oscillation

The Indian monsoon is one of the most consistent and stable features of the global climate system on interannual and interdecadal temporal scales. Area-averaged "all-India" rainfall totals for June–September show a standard deviation that is less than 10% of their long-term (1871–2006) mean. The monsoon's intraseasonal variability (ISV), however, is of considerably larger magnitude; this ISV is hence of crucial importance for rainfall predictions and their social and economic applications (Waliser et al., 1999).

Intraseasonal fluctuations in the monsoon's strength are dominated by a 30–50 day oscillation between periods of enhanced and reduced rainfall over much of the Indian subcontinent, which correspond to maxima in convection over India and the equatorial Indian Ocean (EqIO), respectively (e.g., Yasunari, 1979). These periods are commonly called monsoon "active" and "break" phases. Individual events have been observed to propagate northward from the eastern EqIO (EEqIO) into the Bay of Bengal (BoB) with a speed

of about 1–2° latitude day^{-1} (e.g., Krishnamurti and Subrahmanyam, 1982). The oscillation between active and break events has been frequently termed the northward-propagating intraseasonal oscillation (NPISO). Lawrence and Webster (2002) demonstrated that approximately three-quarters of northward-propagating events also exhibited eastward propagation along the equator. The NPISO is thus thought to be a manifestation of the Madden–Julian Oscillation (Madden and Julian, 1971). Active and break events show a large-scale, organized structure in fields such as outgoing longwave radiation (OLR) and low-level winds (Annamalai and Slingo, 2001). Klingaman et al. (2008b) found that OLR anomalies over India led anomalies of the opposite sign over the EEqIO by six days: active (break) events over India were associated with break (active) events in the EEqIO.

1.2 Atmosphere–ocean interactions in the NPISO

Over the past several years, atmosphere–ocean coupled processes have gained support as a potential mechanism for driving the NPISO. *In-situ* and remotely-sensed observations in the BoB and the Arabian Sea have shown that the passage of individual active and break events were associated with substantial SST variations: the Bay of Bengal Monsoon Experiment (Bhat et al., 2001) and the Joint Air–Sea Monsoon Experiment (Webster et al., 2002) field campaigns measured SST differences of greater than 1°C between individual active and break events. As for the MJO (Woolnough et al., 2000), observations of the NPISO have consistently shown that anomalies in SSTs and rainfall displayed a near-quadrature phase relationship: anomalously warm SSTs preceded enhanced rainfall by approximately 10 days (e.g., Fu and Wang, 2004).

Using National Centres for Environmental Prediction–National Center for Atmospheric Research (NCEP–NCAR) reanalysis, Kemball-Cook and Wang (2001) indicated that anomalies in skin temperature, latent heat flux, and solar radiation moved coherently with anomalous convection. The authors advanced atmosphere–ocean coupled processes as a hypothesis for the northward propagation. Klingaman et al. (2008b) obtained similar results with the ECMWF 40-year reanalysis (ERA-40; Uppala et al., 2005) and SSTs from the Tropical Rainfall Measuring Mission Microwave Imager (TMI). In that study, the authors suggested that SST anomalies provided a critical feedback onto convection by influencing low-level atmospheric stability. Break (active) events generated warm (cold) SST anomalies through enhanced (reduced) insolation and weak (strong) winds, which destabilized (stabilized) the atmosphere ahead of the following active (break) event.

Further indications of the importance of coupled processes come from atmosphere-only GCM (AGCM) simulations. Waliser et al. (2003) concluded that all 10 AGCMs from the Asian-Australian monsoon intercomparison project substantially underestimated the amplitude of the NPISO, despite displaying reasonable seasonal-mean rainfall. Similar studies with individual AGCMs (e.g., Rajendran and Kitoh, 2006) have confirmed this deficiency. AGCMs cannot reproduce the observed near-quadrature phase relationship between SSTs and rainfall; the models too-readily initiate deep convection over the warmest SSTs and suppress convection over the coldest SSTs. Klingaman et al. (2008a) demonstrated that an AGCM could simulate a mean NPISO and individual NPISO events that were similar to observations, if the AGCM were driven with high-resolution observed SSTs that contained realistic amounts of ISV. The SST–convection phase relationship remained incorrect. The NPISO is an intrinsic atmospheric mode; it does not arise from coupled processes, although they may be critical to its maintenance and propagation.

Recent modeling studies have evaluated the impact on the NPISO of including atmosphere-to-ocean feedbacks. Fu and Wang (2004) compared the ECHAM4 AGCM coupled to an intermediate-complexity ocean model to the AGCM alone, forced by the coupled-model SSTs. The improved strength of the NPISO in the coupled simulation implied that the coupled model's ability to generate SST anomalies coherently with atmospheric convection was critical to an accurate simulation of the NPISO. Fu et al. (2007) demonstrated that including air–sea coupling could extend the predictability of the NPISO by about one week. Woolnough et al. (2007) reached similar conclusions for the MJO in the ECMWF monthly forecasting system, with the additional result that coupling to a mixed-layer ocean model with fine vertical resolution improved forecast skill over coupling to a fully dynamic ocean model with coarser vertical resolution. The authors attributed the increased skill of the mixed-layer model to an enhanced sensitivity of the SST to surface fluxes.

1.3 The purpose of the present study

Given the suggested importance of atmosphere–ocean interactions, there is scope to investigate the NPISO in a coupled model with a well-resolved upper ocean. Studies with forced ocean GCMs (OGCMs) have concluded that, for most of the Indian Ocean, the upper-ocean heat budget is determined by thermodynamic processes on intraseasonal temporal scales (e.g., Schiller and Godfrey, 2003). A one-dimensional, purely thermodynamic mixed-layer model may therefore be appropriate for simulating the NPISO. Mixed-layer models are far more computationally economical than fully dynamical OGCMs, which makes the former ideal candidates for use in operational forecasting.

We have assembled a regionally coupled atmosphere–mixed-layer-ocean model—HadKPP—which is described in detail in section 2.1. HadKPP consists of the Hadley Centre Atmospheric Model, version 3 (HadAM3; Pope et al., 2000) coupled to the K Profile Parameterization mixed-layer scheme (KPP; Large et al., 1994). The primary advantages of HadKPP over other coupled models are its fine vertical resolution in the ocean mixed layer; its sub-diurnal coupling frequency; and its fine atmospheric horizontal resolution. We conduct a 30 member ensemble—described in section 2.2—to examine the behavior of the NPISO; we present the results in section 3. Our discussions (section 4) center on the potential for the HadKPP framework to be used for future investigations into the predictability of tropical ISV.

2 Models and Methods

2.1 The HadKPP model

HadAM3 provides the atmospheric component of HadKPP. It is configured as in Pope et al. (2000), except that the horizontal, vertical and temporal resolutions are increased to 1.25° longitude × 0.83° latitude, 30 layers, and 10 minutes, respectively.

The one-dimensional KPP mixed-layer model of Large et al. (1994) provides the ocean component of HadKPP. KPP includes two key non-local effects not commonly found in boundary-layer models: (a) a counter-gradient term in the equation for turbulent diffusion and (b) a dependence of the diffusivity throughout the boundary layer on only the surface forcing and the boundary-layer depth. KPP represents the absorption of solar radiation with the double-exponential formula of Paulson and Simpson (1977), the parameters of which depend on the water's optical properties. All simulations in this study use Jerlov water type IB, which approximates the open ocean (Jerlov, 1976); type IB is used in the Hadley Centre Coupled Model (HadCM3; Gordon et al., 2000).

Bernie et al. (2005) forced KPP with TOGA COARE fluxes in the West Pacific. The authors concluded that a vertical resolution of 1 m and a coupling frequency of 3 hours was necessary to reproduce 90% (95%) of the diurnal (intraseasonal) variability in SSTs observed during TOGA COARE. Woolnough et al. (2007) found that a 1 m vertical resolution in KPP improved the skill of MJO predictions over a 10 m resolution, a behavior that is common in coupled GCMs with fully dynamic ocean models. We configure KPP to have 60 points within a 200 m domain on a stretched grid; there are 39 points in the top 50 m and the surface layer is 0.83 m thick. KPP runs as a matrix of one-dimensional columns, with one column under each HadAM3 grid point.

HadAM3 and KPP exchange coupled fields every 3 hours via the OASIS coupler (Terray et al., 1995). The models are coupled only within 30°S–30°N; 40°E–180°. Outside of this region, HadAM3 is forced by daily climatological SSTs from the National Centre for Ocean Forecasting Forecast Ocean Assimilation Model (FOAM; Bell et al., 2000). FOAM provides three-dimensional daily, global analyses of ocean temperature and salinity on a 1° × 1° horizontal grid. The climatology uses all available FOAM data: 2002–2007.

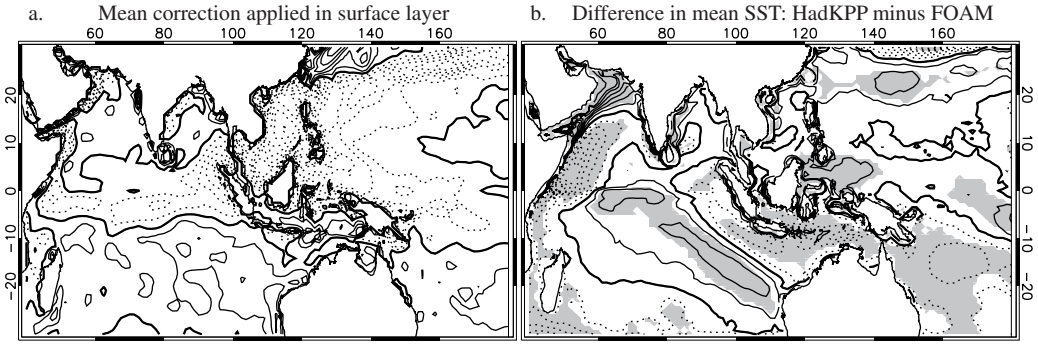

Figure 1: The May–September-mean (a) heat correction (W m^{-2}) applied to HadKPP for the surface layer (0.83 m thick) only; (b) difference in SSTs (°C) for the HadKPP ensemble-mean minus the FOAM climatology (2002–2007). Contours are drawn every (a) 1 W m^{-2}and (b) 0.1°C. Negative contours are dotted; the zero contour is doubly thick.

2.2 HadKPP experiment design

We conduct a 30 member ensemble of May–September HadKPP simulations. This provides a one-month "spin-up" before the 1 June climatological monsoon onset. Each member is initialized with a separate 1 May atmosphere from the HadAM3 ensemble described in section 2.3. KPP is initialized with the FOAM climatological 1 May ocean temperatures and salinity.

Without heat corrections, HadKPP drifts substantially—as much as 1.5°C month^{-1}—from the FOAM climatology due to the lack of ocean heat transport in KPP. To reduce this drift, we apply ocean heat corrections to all ensemble members. The heat corrections are calculated from separate forced integrations of HadAM3 and KPP, using a subset of ten ensemble members chosen randomly. The ten five-month HadAM3 integrations are forced by the climatological FOAM SSTs. The output from each HadAM3 integration is used to drive an integration of KPP. The monthly-mean KPP temperatures are compared to the FOAM climatology; a separate correction is computed for each KPP vertical point at each horizontal grid point. The mean correction applied to the surface layer is shown in Fig. 1a.

The ensemble-mean—from the subset of ten members—monthly-mean heat correction is calculated for each month in May–September and applied to the 30 member, coupled HadKPP ensemble. Using a subset of ensemble members and taking means of the correction over the ensemble and over each month should allow the ensemble to retain intra-ensemble and intra-seasonal variability. As a result of the heat-correction technique, the HadKPP ensemble has biases of only on the order of 0.1°C in its May–September mean SSTs (Fig. 1b).

2.3 The HadAM3 ensemble

In section 3, we compare HadKPP to an ensemble of HadAM3 simulations that was conducted in Klingaman et al. (2008a). HadAM3 was forced globally by daily, observed SSTs from the U. K. Met Office's Operational Sea Surface Temperature and Sea Ice Analysis (OSTIA) product. As with the HadKPP ensemble, the HadAM3 ensemble consists of 30 members. Further details can be found in Klingaman et al. (2008b).

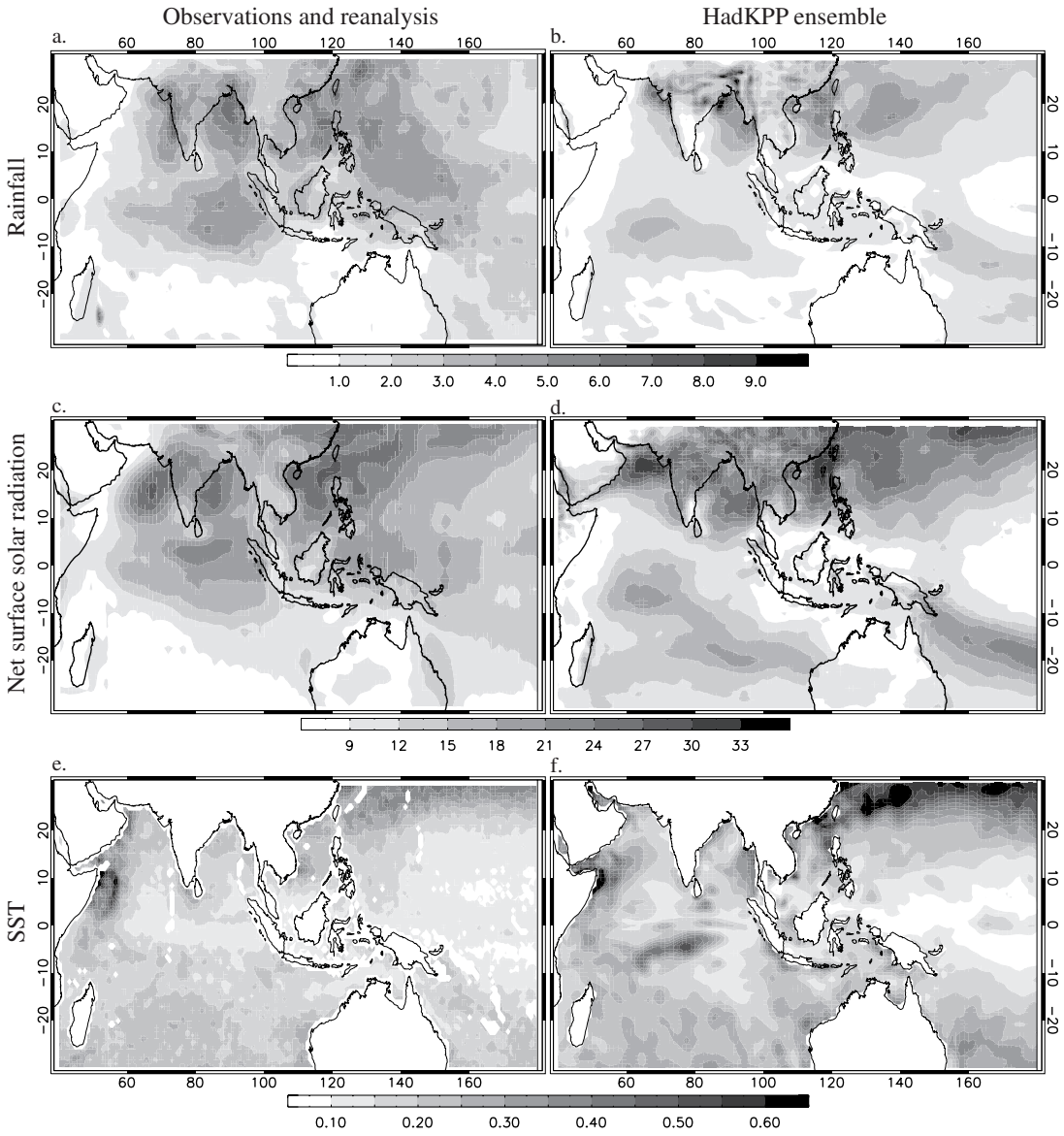

Figure 2: The standard deviation in 30–50 day bandpass-filtered JJA (a,b) rainfall (mm day^{-1}), (c,d) net surface solar radiation (W m^{-2}) and (e,f) SSTs ($^{\circ}$C) from (left) observations and reanalysis and (right) the HadKPP ensemble. Observations and reanalysis used are (a) GPCP (1998–2007), (c) TMI (1998–2007) and (e) ERA-40 reanalysis (1957–2002).

3 Results

3.1 Intraseasonal variability

To examine ISV in HadKPP and observations and reanalysis, we compute the standard deviation in 30–50 day bandpass-filtered June–August (JJA) rainfall, net surface solar radiation and SST. The data are restricted to JJA due to edge effects of the bandpass filter.

In the 1° × 1° Global Precipitation Climatology Program (GPCP) analyses, maxima in ISV in rainfall occur in the EEqIO, the BoB and the northwestern tropical Pacific (Fig. 2a). This is consistent with past studies based on observations and reanalysis, which have found that the NPISO is most pronounced in the eastern half of the Indian Ocean basin and the West Pacific (e.g., Klingaman et al., 2008b). While the HadKPP ensemble

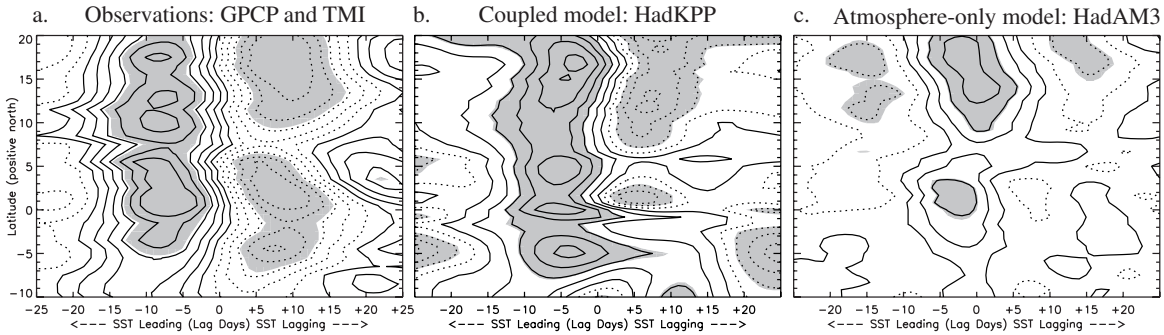

Figure 3: Lead–lag correlations between the linear trend (using an 11-day centered window) in longitude-averaged (80–90°E) June–September SST and rainfall for (a) GPCP and TMI, (b) HadKPP and (c) HadAM3. Contours are drawn every 0.1; negative contours are dotted. Gray shading indicates statistical significance at the 5% level.

produces similar ISV to GPCP off the equator in the Northern Hemisphere, HadKPP has far less ISV than GPCP along the equator (Fig. 2b). Inness and Slingo (2003) found low equatorial ISV in convection during northern winter in both HadCM3 and HadAM3. The HadAM3 ensemble (section 2.3) exhibits a similar spatial pattern of rainfall ISV to HadKPP (not shown). The low ISV on the equator is a deficiency in the atmospheric model; it is not affected—positively or negatively—by coupling.

HadKPP also suffers from limited equatorial ISV in net surface solar radiation (SSR_{net}), which supports the hypothesis that the low rainfall variability is due to deficiencies in the atmospheric convection scheme. When compared to the ISV in the ERA-40 reanalysis (Fig. 2c), HadKPP again has adequate amounts of ISV in SSR_{net} off the equator in the Northern Hemisphere, but less than 50% of the ISV from ERA-40 in the EEqIO and in the equatorial West Pacific (Fig. 2d). As for rainfall, the lack of ISV in SSR_{net} is not limited to HadKPP: the ISV from the HadAM3 ensemble is similar to that from HadKPP (not shown).

Analysis of the ISV in TMI SSTs demonstrates that local maxima occur along the Somali coast—a region of strong low-level winds during JJA—at the head of the BoB and in the subtropical West Pacific (Fig. 2e). In general, HadKPP produces similar amounts of ISV in SSTs to TMI in regions in which HadAM3 provides adequate ISV in SSR_{net}, compared to ERA-40. Thus, HadKPP produces accurate amounts of ISV in SSTs in the BoB, along the Somali coast and in the Arabian Sea (Fig. 2f). The converse is also true: HadKPP produces incorrect ISV in SSTs where the ISV in SSR_{net} is incorrect. HadKPP overestimates the ISV in SSTs the northwestern tropical Pacific, where the ISV in SSR_{net} is also overestimated. ISV in SSTs in the equatorial West Pacific and around the Maritime Continent is reduced by more than half in HadKPP, compared to TMI. While the equatorial Indian and Pacific Oceans contain low ISV when the entire season is considered, our analysis in section 3.2 will demonstrate that during strong NPISO events the equatorial SST anomalies can be nearly as strong as those in the BoB. Woolnough et al. (2001) found that the majority of the surface forcing on SSTs during the MJO came from SSR_{net}; these results support that conclusion.

Coupling to KPP improves the phase relationship between SSTs and rainfall, compared to observations. As mentioned in section 1.2, observations have shown that warm (cold) SSTs precede (follow) heavy rainfall by approximately 10 days (Fig. 3a). Here, the phase relationship is calculated as the correlation between the linear trend in rainfall and SSTs that were first longitude-averaged over the eastern Indian Ocean (80–90°E), in which the NPISO is strongest (e.g., Klingaman et al., 2008b). The linear trend uses an 11-day centered window and so acts as a limited-width lowpass filter; Klingaman et al. (2008a) used this technique to highlight ISV.

At most latitudes in HadKPP, SSTs lead rainfall by 5–8 days (Fig. 3b), which is shorter than the 8–10 days suggested by GPCP and TMI. This may be due to the HadAM3 convection scheme being overly sensitive to SST anomalies, despite the presence of coupled feedbacks. It may also be due to the lack of horizontal advection in the one-dimensional KPP model, which may cause an accelerated increase in SSTs that would

trigger convection more quickly. The authors plan to analyze a HadCM3 integration to investigate whether coupling to a fully-dynamic ocean model improves this phase relationship. HadKPP clearly produces a more-accurate phase relationship than HadAM3, in which the model too-readily generates deep convection and heavy rainfall over the warmest prescribed SSTs (Fig. 3c; Klingaman et al., 2008a).

3.2 Composite NPISO events

In this section, we construct composite active and break events to compare HadKPP with observations; for brevity, only the results from composite active event will be discussed. Separate composites are constructed for HadKPP and for observations; the latter composite uses GPCP rainfall and TMI SSTs.

Active and break events are defined using a modified version of the "two-box" technique described in Klingaman et al. (2008b). The two boxes encompass the dominant centers of NPISO activity, as described in section 1.1 and Figs. 2a and 2b: the central Indian subcontinent ("Box I": 70–90°E; 15–25°N) and the equatorial Indian Ocean ("Box EqIO": 65–90°E; 10°S–5°N). First, rainfall is area-averaged in each box. Using an 11 day centered window, the linear trend in the area-averaged rainfall is calculated for each day in 20 June–10 September. The first and final 20 days of the climatological monsoon season are excluded so as not to include the monsoon onset (retreat) as an active (break) event. The intraseasonal index is calculated as the trend in Box I minus the trend in Box EqIO. An active event is defined as a period in which the intraseasonal index is greater than its mean plus one standard deviation for at least five consecutive days.

The 30 HadKPP ensemble members contain 33 active events with a mean length of 8.0 days. The 1998–2007 GPCP analyses contain 15 active events with a mean length of 8.1 days; GPCP produces almost 50% more active events per season than HadKPP. The events are centered on the date that the index first exceeds its mean plus one standard deviation; this is "day 0". Day 0 therefore represents the beginning of active (break) conditions over India (the EqIO). Days with negative (positive) numbers occur before (after) day 0. Fig. 4 presents composite triad-mean rainfall and SST anomalies for the observed and HadKPP composite active events. "Triad 0" is the mean of day -1, day 0 and day +1; "triad +1" is the mean of day +2, day +3 and day +4; and so on. The composite anomalies are the arithmetic mean of the anomalies for the individual events. Anomalies are taken from a daily climatology, which for HadKPP is the ensemble mean. A 30 day lowpass filter is applied to the daily climatology to remove high-frequency variability.

In the observed active composite, triad -4 (i.e., about 12 days before the active event begins over India) is characterized by a break event over the subcontinent and an active event in the EqIO. The equatorial active event moves east in triad -3 and develops a northwest–southeast tilted structure in triad -2, while the Indian break event dissipates. The active event continues to propagate north in triad -1 and extends onto the Indian subcontinent and into the Arabian Sea by triad 0. Meanwhile, a break event forms in the EqIO in triad -1, moves east in triad 0, and intensifies in the EEqIO in triad +1. This break event moves north in triads +2 and +3, reaching southwest India in triad +4.

TMI SSTs reveal that the observed active composite is associated with SST anomalies of up to $\pm$ 0.4°C on the equator and in the BoB. As suggested in Fig. 3a, these SST anomalies are out of phase with the GPCP rainfall, such that warm SST anomalies peak in the northern BoB in triad -2, 9–12 days before heavy rainfall begins there in triads +1 and +2. Similarly, cold SST anomalies of up to -0.3°C are found in the EqIO in triads -3 and -2, 6–9 days before the break event begins there.

Compared to the observed composite, the HadKPP composite displays rainfall anomalies of the correct sign and similar magnitude over India, but smaller anomalies over the EqIO and little northward propagation. HadKPP also has very limited SST anomalies on the equator, to the point where they are practically non-existent. While the HadKPP and observed composites agree in rainfall in triad -4, HadKPP does not reproduce the observed eastward movement of the equatorial active event in triad -3 and triad -2. The active event reappears in HadKPP only in triad 0 over India, which is specified by the index used to create the composite. The equatorial break event appears in triad 0, but it also fails to propagate north to India, instead dissipating in the EEqIO. The

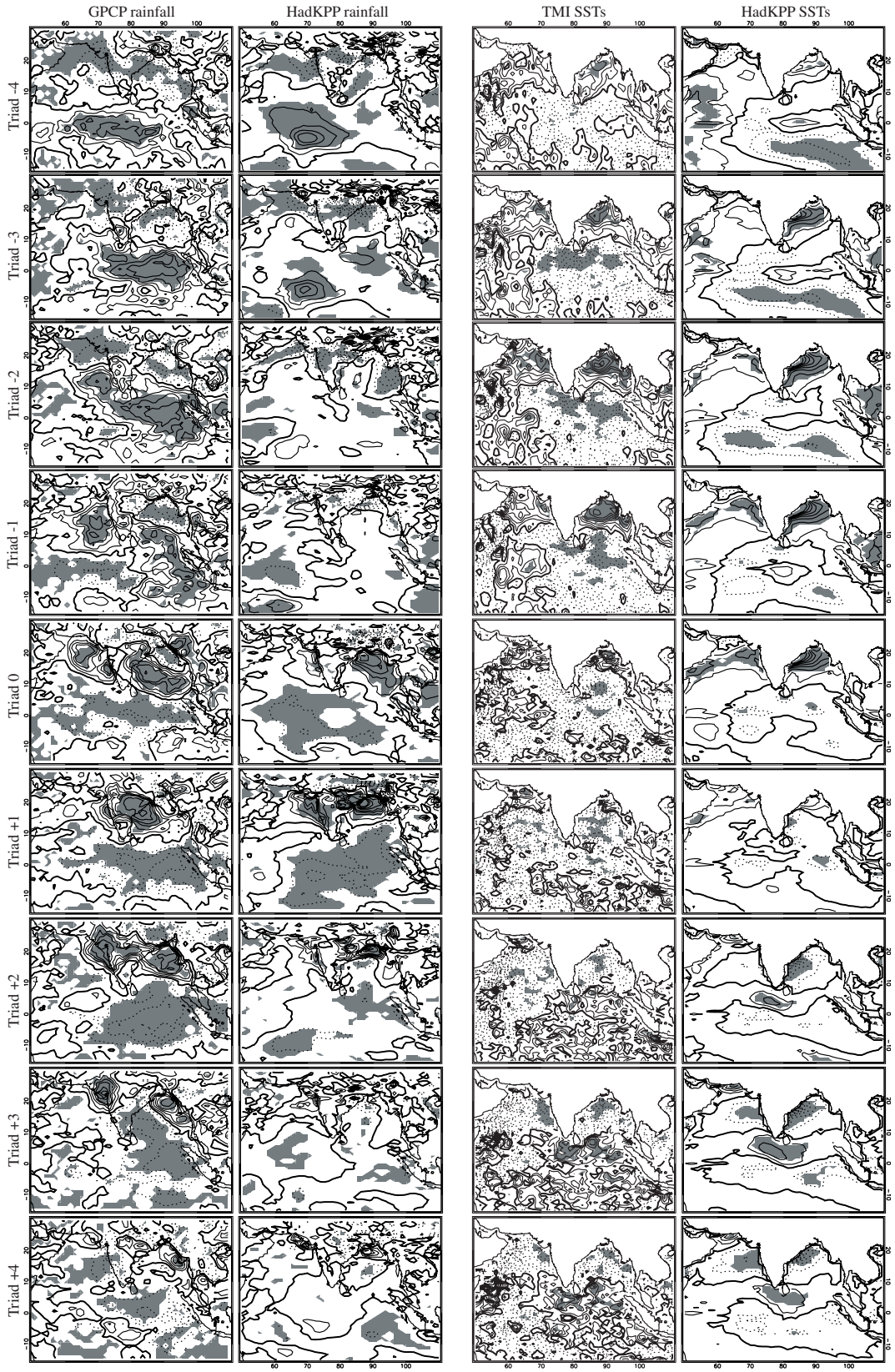

Figure 4: Triad-mean anomalies for the composite active event. Contours for rainfall are drawn every 2 mm day^{-1}from $\pm$2 mm day^{-1}until $\pm$12 mm day^{-1}, then every 4 mm day^{-1}. Contours for SST are drawn every 0.05°C. Negative contours are dotted; the zero contour is doubly thick. Gray shading indicates statistical significance at the 5% level using a Student's t test.

NPISO in HadKPP therefore appears as a standing oscillation between the EqIO and India, rather than as the large-scale, coherent, northward-propagating active events seen in observations.

HadKPP does, however, reproduce very well the TMI SST anomalies in the BoB, with respect to both their magnitude and their timing with respect to anomalous rainfall. Warm anomalies appear in the northwestern Bay of Bengal during the Indian break event in triad -3, then intensify and expand in triad -2 and triad -1 in a manner consistent with TMI. Cold SST anomalies appear in triad +2 and persist through triad +4, again consistent with TMI. When combined with the lack of equatorial SST variability, this behavior reinforces the conclusion of section 3.1: when provided adequate atmospheric forcing on intraseasonal temporal scales, as in the Bay of Bengal, KPP generates accurate SST anomalies with respect to observations; limited ISV in atmospheric fluxes on the equator results in limited SST anomalies there. The lack of equatorial ISV in HadAM3, therefore, is likely the ultimate cause of the deficiencies in the NPISO in HadKPP.

4 Summary and discussion

HadKPP holds promise as a coupled-model framework capable of exploring the predictability of the NPISO and other intraseasonal phenomena (e.g., the MJO). HadKPP includes a computationally inexpensive mixed-layer ocean model capable of running at fine vertical resolution and with three-hourly coupling, both of which have been shown to improve the ISV of tropical SSTs (e.g., Bernie et al., 2005; Woolnough et al., 2007).

Although previous studies have highlighted the importance of atmosphere–ocean coupling in modeling the NPISO (e.g., Fu and Wang, 2004), this study has shown that coupling alone is not a panacea for model deficiencies in representing ISV. The most glaring deficiency in HadKPP is the limited equatorial ISV in net surface solar radiation (Fig. 2d). This is solely the fault of the atmospheric model, HadAM3, and is not limited to northern summer (Inness and Slingo, 2003). The presence of atmosphere–ocean interactions alone cannot ameliorate this type of error. Simply put, atmosphere-to-ocean feedbacks are of little value if the atmospheric model cannot diagnose fluxes of the magnitude required to substantially modify the SSTs.

This lack of variability in surface fluxes in the EqIO contributes strongly to the weak NPISO in HadKPP. As a purely thermodynamic, one-dimensional model, KPP simply cannot create SST anomalies on temporal scales at which there is little variability in the atmospheric forcing. In a comparison of HadAM3 ensembles forced by daily and monthly-mean observed SSTs, Klingaman et al. (2008a) demonstrated that a lack of ISV in SSTs inevitably feeds back onto a lack of variability in convection and creates a weak NPISO. Coupled feedbacks likely degrade the representation of NPISO events in HadKPP, therefore, as an initial lack of ISV in equatorial convection weakens SST variability, which in turn further diminishes the ISV in convection. The ultimate cause of the errors in the NPISO simulation lies with the HadAM3 convection scheme, however, not with KPP.

In spite of these errors, HadKPP produced an intraseasonal oscillation that was similar to observations in three key respects: the magnitude and spatial distribution of rainfall anomalies over India, the magnitude and timing of SST anomalies in the BoB and the Arabian Sea and the SST–convection phase relationship. The latter two are perhaps the most important indications of the model's potential for exploring the predictability of tropical ISV. In regions where the atmosphere provided sufficient forcing (e.g., the BoB), KPP was able to generate SST anomalies that agreed very well with those from the high-resolution TMI analyses. These SST anomalies were not only of the correct magnitude, but they demonstrated the correct phase relationship with the rainfall anomalies over India in the GPCP analyses. High-frequency, high-magnitude SST anomalies have been shown to be critical to the development of convection on intraseasonal temporal scales in GCM (Klingaman et al., 2008a). This study has demonstrated that, at least in the BoB, such anomalies can be generated with a mixed-layer model using fine vertical resolution. This reinforces the conclusion of Schiller and Godfrey (2003) that thermodynamic processes control the upper-ocean heat budget of the Indian Ocean on intraseasonal temporal scales. This conclusion is critical for numerical weather prediction: intraseasonal SST anomalies may be predicted accurately via coupling to an economical, thermodynamic ocean, rather than to an expensive, fully dynamical ocean.

Indian agriculture requires a 14–21 day lead time to respond to forecasts of the NPISO (Webster and Hoyos, 2004). This is longer than the persistence time of SST anomalies (Fig. 4), which suggests that the current operational forecasting framework of an AGCM with persisted SST anomalies will not be useful. Coupled atmosphere–mixed-layer-ocean models provide a computationally efficient means to include atmosphere-to-ocean feedbacks and predict the SST anomalies that are critical to the evolution of the intraseasonal oscillation.

Acknowledgments

Dr. Jeff Cole of the National Centre for Atmospheric Science Computational Modeling Support group provided assistance with assembling HadKPP. All integrations were performed using HPCx, the UK's national high-performance computing service. The GPCP combined precipitation data were provided by the NASA/Goddard Space Flight Center's Laboratory for Atmospheres. ERA-40 reanalysis was provided by the European Centre for Medium-Range Weather Forecasts via an archive at the University of Reading Department of Meteorology. The TMI microwave optimally-interpolated SST data were produced by Remote Sensing Systems.

References

Annamalai, H. and J. M. Slingo, 2001: Active/break cycles: Diagnosis of the intraseasonal variability of the Asian summer monsoon. *Clim. Dynam.*, **18**, 85–102.

Bell, M. J., R. M. Forbes, and A. Hines, 2000: Assessment of the FOAM global data assimilation system for real-time operational ocean forecasting. *J. Mar. Sys.*, **25**, 1–22.

Bernie, D. J., S. J. Woolnough, and J. M. Slingo, 2005: Modeling diurnal and intraseasonal variability of the ocean mixed layer. *J. Climate*, **18**, 1190–1202.

Bhat, G. S. et al., 2001: BOBMEX: The Bay of Bengal Monsoon Experiment. *Bull. Amer. Meteorol. Soc*, **82**, 2217–2243.

Fu, X. and B. Wang, 2004: The boreal-summer intraseasonal oscillations simulated in a hybrid coupled atmosphere-ocean model. *Mon. Wea. Rev.*, **132**, 2628–2649.

Fu, X., B. Wang, D. E. Waliser, and L. Tao, 2007: Impact of atmosphere-ocean coupling on the predictability of monsoon intraseasonal oscillations. *J. Atmos. Sci.*, **64**, 157–174.

Gordon, C., C. Cooper, C. A. Senior, H. Banks, J. M. Gregory, T. C. Johns, J. F. B. Mitchell, and R. A. Wood, 2000: The simulation of SST, sea ice extents and ocean heat transports in a version of the Hadley Centre coupled model without flux adjustments. *Clim. Dynam.*, **16**, 147–168.

Inness, P. M. and J. M. Slingo, 2003: Simulation of the Madden–Julian oscillation in a coupled general circulation model. Part I: Comparison with observations and an atmosphere-only GCM. *J. Climate*, **16**, 345–364.

Jerlov, N. G., 1976: *Marine optics*. Elsevier, New York City, New York, 231 pp.

Kemball-Cook, S. and B. Wang, 2001: Equatorial waves and air-sea interaction in the boreal summer intraseasonal oscillation. *J. Climate*, **14**, 2923–2942.

Klingaman, N. P., P. M. Inness, H. Weller, and J. M. Slingo, 2008a: The importance of high-frequency sea-surface temperature variability to the intraseasonal oscillation of Indian monsoon rainfall. *Journal of Climate*, In press.

Klingaman, N. P., H. Weller, J. M. Slingo, and P. M. Inness, 2008b: The intraseasonal variability of the Indian summer monsoon using TMI sea-surface temperatures and ECMWF reanalysis. *Journal of Climate*, **21**, 2519–2539.

Krishnamurti, T. N. and D. Subrahmanyam, 1982: The 30–50 day mode at 850 mb during MONEX. *J. Atmos. Sci.*, **39**, 2088–2095.

Large, W., J. McWilliams, and S. Doney, 1994: Oceanic vertical mixing: A review and a model with a nonlocal boundary layer parameterization. *Rev. Geophys.*, **32**, 363–403.

Lawrence, D. M. and P. J. Webster, 2002: The boreal intraseasonal oscillation: Relationship between northward and eastward movement of convection. *J. Climate*, **59**, 1593–1606.

Madden, R. A. and P. R. Julian, 1971: Detection of a 40–50 day oscillation in the zonal wind in the tropical Pacific. *J. Atmos. Sci.*, **28**, 702–708.

Paulson, C. A. and J. J. Simpson, 1977: Irradiance measurements in the upper ocean. *J. Phys. Oceanogr.*, **7**, 952–956.

Pope, V. D., M. L. Gallani, P. R. Rowntree, and R. A. Stratton, 2000: The impact of the new physical parameterizations in the Hadley Centre climate model. *Clim. Dynam.*, **16**, 123–146.

Rajendran, K. and A. Kitoh, 2006: Modulation of tropical intraseasonal oscillations by atmosphere-ocean coupling. *J. Climate*, **19**, 366–391.

Schiller, A. and J. S. Godfrey, 2003: Indian Ocean intraseasonal variability in an ocean general circulation model. *J. Climate*, **16**, 21–39.

Terray, L., E. Sevault, E. Guilyardi, and O. Thual, 1995: The OASIS coupler user guide version 2.0. Technical Report TR/CMGC/95-46, CERFACS.

Uppala, S. M. et al., 2005: The ERA-40 re-analysis. *Q. J. R. Meteorol. Soc.*, **131**, 2961–3012.

Waliser, D. E., C. Jones, J. K. Schemm, and N. E. Graham, 1999: A statistical extended-range tropical forecast model based on the slow evolution of the Madden-Julian oscillation. *J. Climate*, **12**, 1918–1939.

Waliser, D. E. et al., 2003: AGCM simulations of intraseasonal monsoon variability associated with the Asian summer monsoon. *Clim. Dynam.*, **21**, 423–446.

Webster, P. J. and C. Hoyos, 2004: Prediction of monsoon rainfall and river discharge on 15–30-day time scales. *Bull. Am. Meteor. Soc.*, **85**, 1745–1765.

Webster, P. J. et al., 2002: The JASMINE pilot study. *Bull. Amer. Meteorol. Soc.*, **83**, 1603–1630.

Woolnough, S. J., J. M. Slingo, and B. J. Hoskins, 2000: The relationship between convection and sea surface temperatures on intraseasonal timescales. *J. Climate*, **13 (12)**, 2086–2104.

———, 2001: The organization of tropical convection by intraseasonal sea surface temperature anomalies. *Q. J. R. Meteorol. Soc.*, **127**, 887–907.

Woolnough, S. J., F. Vitart, and M. A. Balmaseda, 2007: The role of the ocean in the Madden–Julian Oscillation: Implications for MJO prediction. *Quart. J. R. Meteorol. Soc.*, **133**, 117–128.

Yasunari, T., 1979: Cloudiness fluctuations associated with the Northern Hemisphere summer monsoon. *J. Meteor. Soc. Japan*, **57**, 227–242.